ACS NANO
Cite This: ACS Nano 2017, 11, 12615–12623
www.acsnano.org

ARTICLE

Detecting Interactions between Nanomaterials and Cell Membranes by Synthetic Nanopores

Binquan Luan,*,† Shuo Zhou,‡ Deqiang Wang,‡ and Ruhong Zhou*,†

†Computational Biology Center, IBM Thomas J. Watson Research, Yorktown Heights, New York 10598, United States
‡Chongqing Institute of Green and Intelligent Technology, Chinese Academy of Sciences, Chongqing 400714, China

Supporting Information

ABSTRACT: **Engineered nanomaterials have been increasingly utilized in industry for various consumer products, environmental treatments, energy storage, and biomedical applications. Meanwhile, it has been established that certain nanomaterials can be toxic to biological cells from extensive experimental and theoretical studies. Despite that the exact molecular mechanisms of this nanomaterial toxicity are still not well understood, it is ubiquitous that their interactions with cell membranes, through either endocytosis or penetration (and thus potential lysis), act as the first step toward the inflammation or even the death of a cell. To facilitate the study of nanomaterial−membrane interactions, here we demonstrate a nanopore-based single-molecule approach that can be applied to monitor a specific nanomaterial−membrane interaction in real time. Combined with molecular dynamics and experimental approaches, we show how an ionic current can be used to detect membrane damage by a graphene nanosheet and illustrate the underlying molecular mechanism. More generally, we expect that measured transmembrane ionic currents (both DC and AC) can signify many particle-induced membrane modifications, such as hole formation, particle adsorption, and protein insertion.**

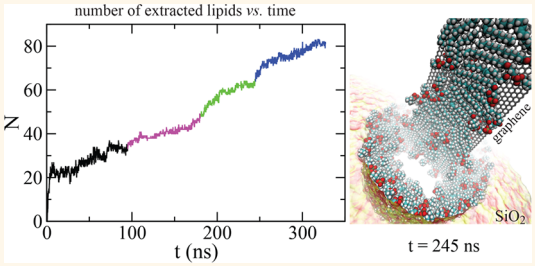

KEYWORDS: *bionano, nanotoxicity, nanopore, biosensor, membrane damage, graphene, nanomaterials*

The membrane of a biological cell encloses cytoplasm, such as cytosol and organelles, and protects the cell from its extracellular environment. Functionally, the membrane regulates the transport of nutrients into and wastes out of a cell. The damage of a cell membrane can often lead to the leakage of intracellular substances (*e.g.*, ions, mRNA, and proteins), which may trigger necrosis for cellular death. During bacterial infection that targets a cell membrane, protein toxins (also known as pore-forming-proteins, such as α-hemolysin from *Staphylococcus aureus*[1]) can self-assemble into a transmembrane channel on the host membrane, causing cell lysis or leakage, which is the major mechanism for cellular damage.[2] Associated with Alzheimer's disease (a deadly neurodegeneration disease), amyloid-β 42 peptides (Aβ42), which are intrinsically disordered, can surprisingly aggregate on a cell membrane and form pores with various sizes.[3,4] Recently, the same concept or mechanism has been applied to the design of synthesized antibacterial drugs. For example, positively charged peptides or polymers can target the negatively charged bacterial membrane and effectively kill bacteria by forming holes on their membrane.[5−7]

Engineered nanomaterials have been commercially used in cosmetics, catalysis, microelectronics, food, and drug industries, due to their attractive physical and chemical properties. However, this is accompanied by growing concerns on nanomaterials' biocompatibility (*i.e.*, potential harmful interactions with biological systems).[8,9] Some nanomaterials have been known to induce cytotoxicity to biological cells by damaging cell membranes, similar to protein toxins and amyloid peptides. For example, hydrophobic nanomaterials of particular sizes can penetrate into a cell membrane directly (a passive transport in contrast to endocytosis) and leave open pores in the bilayer.[10] A poly(methacrylic acid) (PMAA) coated gold nanoparticle (AuNP) can promote the initial adsorption on a lipid membrane and later abduct a patch of membrane lipids leaving a large hole in the bilayer.[11] Additionally, graphene nanosheets have been shown to aggressively extract lipids out of a cell membrane,[12,13] causing damage to the membrane.

The adsorption of a nanoparticle on a supported lipid bilayer,[14] followed by possible damage to the membrane, can be experimentally monitored using atomic force microscopy (AFM)[15] or a quartz crystal microbalance with dissipation (QCM-D).[11,16] Alternatively, pore formation as a consequence of interactions between nanomaterials and vesicles (with molecular dyes inside) can be discovered by applying fluorescence techniques to optically measure dye leakage.[17]

Received: October 2, 2017
Accepted: November 21, 2017
Published: November 21, 2017

DOI: 10.1021/acsnano.7b07005
ACS Nano 2017, 11, 12615–12623

To facilitate and simplify experimental detection of nanomaterial–membrane interactions, here, we propose a nanopore-based single-molecule technique that has been widely used to detect biomolecules (such as DNA[18] and proteins[19]) electrochemically. Similar to a black lipid membrane (BLM)[14] at macroscale, a patch of lipid bilayer is self-assembled inside a nanometer-sized pore (or generally <1 μm) drilled through a thin (~5 nm) solid-state (*e.g.*, SiO_2) membrane. For simplicity, lipids outside the pore due to lipid-spanning are not modeled. In a typical fluidic device, such a membrane separates the *cis* and *trans* fluidic chambers, with an external electric field E applied normal to the membrane (Figure 1a). After loading the

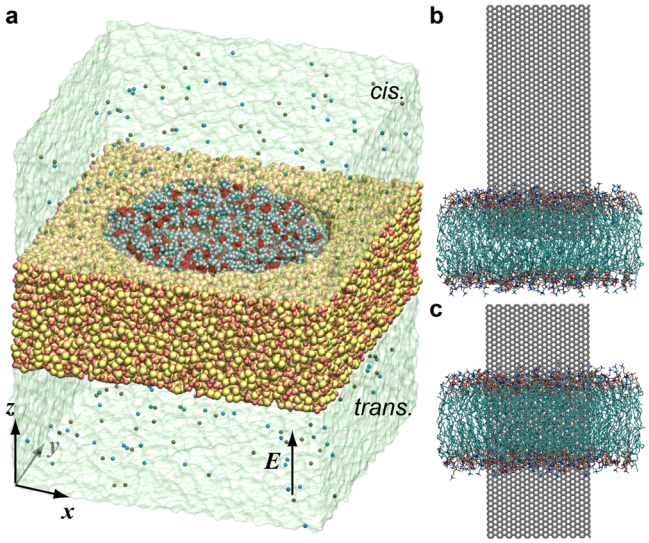

Figure 1. Setup of molecular dynamics (MD) simulations. (a) The nanopore system; Si and O atoms in the solid-state nanopore are shown in yellow and red; the POPC lipids filling the nanopore are shown as van der Waals spheres; K^+ and Cl^- are represented as tan and cyan dots; water is shown transparently. (b) A graphene nanosheet enters halfway through the membrane (Sim-1). (c) A graphene nanosheet enters the membrane entirely and is "symmetrically docked" on the membrane with equally exposed segments on both sides of the membrane (Sim-2).

to-be-tested nanomaterials in the electrolyte on the *cis* side, it is expected that the potential nanomaterial–membrane interactions can be conveniently monitored by measuring the ionic currents through the membrane.

To prove the principle, we carried out molecular dynamics (MD) simulations on the potential harmful effects resulting from a graphene nanosheet's interaction with the lipid bilayer supported by the solid-state nanopore. The MD method has been extensively applied in studying both biomolecules[20−23] and nanotechnologies.[24−27] Previously, MD simulations have shown that a graphene nanosheet can spontaneously insert into a lipid bilayer through its sharp edges and corners,[12,13] destructively extracting lipids out of the membrane.[12,28] Recently, through both experimental and simulation approaches, it was demonstrated that the extensive loss of lipids due to the extraction by a graphene nanosheet may eventually yield a hole in the membrane.[17,29] Here, we focus on the dynamic graphene–membrane interactions after graphene's insertion and show how the nanopore sensor can be used to detect the hole-formation in the membrane. Generally, this method can be applied to study interactions between a cell membrane and many other engineered nanomaterials, providing a means for evaluating their nanotoxicity *in vitro*.

RESULTS AND DISCUSSION

The simulation system for nanopore-based assessments of potential nanotoxicity of nanomaterials toward a cell membrane is illustrated in Figure 1. Briefly, to obtain the SiO_2 nanopore *in silico*, atoms in the solid membrane were fully mixed at a high temperature before being quenched to 300 K. During the quenching process, atoms within 5 nm of the z axis were harmonically pushed out, forming a cylindrical channel. Finally, the system was equilibrated at 1 bar and 300 K, with the periodic boundary condition applied in the x- and y-directions only. The thickness of the equilibrated membrane is about 5 nm.

A patch of pre-equilibrated 1-palmitoyl-2-oleoyl-*sn*-glycero-3-phosphocholine (POPC) lipid bilayer was placed inside a 10 nm diameter nanopore (D = 10 nm). Previous studies[30] have shown that such membrane model can yield insightful understanding of the interactions between nanomaterials and a cell membrane. The membrane complex was further solvated in a 0.15 M KCl electrolyte (Figure 1a), separating the electrolyte into *cis* and *trans* fluidic chambers. After minimization and equilibration, the lipid density in the POPC membrane is about one lipid per 67.7 Å^2, which is comparable to that measured in experiment.[31] Experimentally, the critical biasing voltage is 0.3 V, below which electroporation does not occur, for example, a typical voltage of 0.15 V used for monitoring the ssDNA translocation through an α-hemolysin channel in a supported lipid bilayer.[18] In simulation, due to the force field[32] (describing POPC lipids), a much larger baising voltage (*e.g.*, 2 V) is required for the poration.[33] Here, we applied a biasing electric voltage of 0.5 V across the entire system (height ~16 nm), ensuring that no electroporation can occur in our simulations.

As shown in previous studies, a graphene nanosheet spontaneously enters a cell membrane through its sharp edges;[12,13] here we focus on possible subsequent membrane damages after graphene's entry into the cell membrane. Two docking positions of a graphene nanosheet in the membrane were investigated: (1) a graphene nanosheet (63.8 × 136.3 Å^2) enters only the upper layer of the membrane (Figure 1b), referred to as Sim-1 hereafter; (2) the same graphene nanosheet penetrates the bilayer and is "symmetrically docked" on the membrane with equally exposed segments on both sides of the membrane (Figure 1c), referred to as Sim-2 hereafter. In both cases, the graphene nanosheet was perpendicular to the membrane surface, with its position fixed during all simulations. Positions of the lipids that are in conflict with the graphene nanosheet were slightly moved or reoriented, and the top view of an inserted graphene nanosheet after minimization and equilibration is shown in Figure S1 in the Supporting Information.

Due to the strong van der Waals interaction, as well as hydrophobic interaction (due to water), between lipids and the graphene nanosheet, consistent with previous studies,[12,28] we also observed the vigorous extraction of lipids toward the graphene surface. In Sim-1, since the graphene nanosheet only partially penetrated into the membrane, the strong lipid-graphene interaction drove the entire membrane to bend toward the graphene after a few nanoseconds (Figure S2a), allowing the lower layer of the lipid membrane to cover the graphene nanosheet as well. After that, the process of lipid-

DOI: 10.1021/acsnano.7b07005
ACS Nano 2017, 11, 12615−12623

extraction toward the graphene nanosheet (exposed in the *cis* chamber) started and the number of extracted lipids increased with time as shown in Figure 2a. In Sim-2, because the

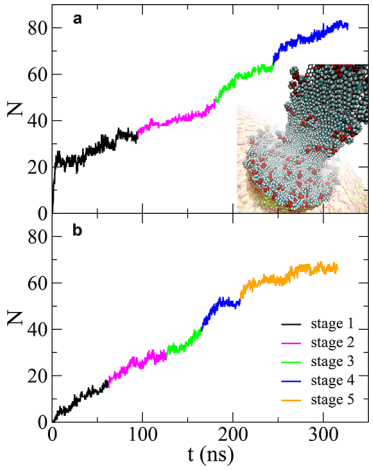

Figure 2. Time-dependent number of POPC lipids extracted onto the graphene nanosheet in Sim-1 (a) and in Sim-2 (b).

graphene nanosheet was fully inserted, lipids were allowed to be extracted toward graphene fragments in both *cis* and *trans* chambers (Figure 2b, Figure S2b).

In these proof-of-principle simulations, we modeled a small graphene nanosheet that can only be covered by 30 to 40 lipids. For example, at around 100 ns in Sim-1 (the end of the black line in Figure 2a), the exposed graphene nanosheet was fully covered by extracted lipids (see inset in Figure 2a). To model the toxic effect by a larger nanosheet, we divided the entire simulation into several stages. In order to continue extracting lipids, at the end of each stage all extracted lipids covering the exposed nanosheet were removed from the simulation system. After proper equilibration in the NPT ensemble for 0.5 ns with all heavy (non-hydrogen) atoms in lipids restrained, the simulation resumes in the NVT ensemble in the next stage. We carried out four and five simulation stages in Sim-1 and Sim-2, respectively. Due to the removal of extracted lipids, the dimension (along z axis) of the simulation box were slightly reduced in latter stages, *e.g.* 16.35, 16.07, 15.90, and 15.80 nm in stages 1−4 in Sim-1. Thus, this simulation approach allows us to investigate the depenency of graphene's size on the pore formation (see below).

Overall, the rates of lipid extraction in Sim-1 and Sim-2 are comparable, as shown from the slopes (dN/dt) of the lines in Figure 2. Roughly, one lipid was extracted every 4 to 5 ns. This rate is comparable to the result reported under a similar condition in the previous study[12] without applying the electric field, suggesting that the applied electric field barely affected the lipid-extraction process. However, both systems behaved quite differently during the beginning stage. The fast extraction at the beginning of Sim-1 was facilitated by the initial bending of the entire membrane toward the graphene nanosheet in the *cis* chamber. Energetically, the lower lipid−lipid interaction energy in the bent membrane (with an increase surface area) yields the faster lipid-extraction process in Sim-1 in the beginning. In later stages, the lipid extraction in Sim-2 was slightly faster because lipids can be extracted from both sides of the membrane.

Destructive and vigorous extraction of lipids from the membrane would inevitably damage the membrane after some time. Therefore, the above lipid-extraction process can be monitored conveniently by measuring the ionic current through the lipid membrane. From the trajectories of Sim-1 and Sim-2, we calculated the time-dependent ionic currents $I = \sum(q_i v_i)/H$, where H is the system height; q_i and v_i are the charge and the velocity of an *ith* ion, respectively. At the beginning the membrane was not damaged, so the average trans-membrane current was zero as shown in Figure 3.

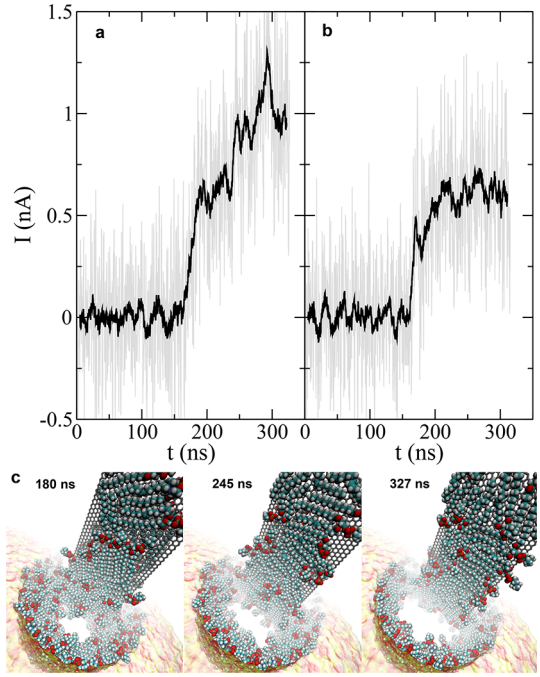

Figure 3. Ionic currents through the nanopore during the Sim-1 (a) and the Sim-2 (b). Gray lines, currents averaged over 1 ns intervals; black lines, currents averaged over 10 ns intervals. (c) Snapshots of the hole-formation in the lipid membrane in Sim-1.

Even after the lipid extraction started, in the early stages, the membrane spanned the entire nanopore despite the loss of lipids. Thus, the ionic current did not increase immediately after the lipid-extraction process occurred. Figure 3 shows that in both Sim-1 and Sim-2, the average current remained at zero for about 160 ns, during which about 40 lipids were extracted onto the graphene nanosheet (Figure 2a). After this critical point ($t \sim 160$ ns), currents in both simulations surged to about 0.5 nA, indicating a significant amount of ions permeated through the lipid membrane. From the trajectory analyses of both systems, a hole was observed in the damaged membrane, which increased its size over time(Figure 3c, and see movie S1 in Supporting Information). Consistently, the hole formation in the damaged membrane in either Sim-1 or Sim-2 occurred after about the same amount of lipids (~40) were extracted. In the current simulation setup, there were a total of 234 lipids in the membrane. Therefore, our results suggest that a hole can form after the membrane loses about 17% of its lipids, which also sets the size limit for a graphene nanosheet in order to produce a pore in the membrane. In a live cell, due to the diffusion of excess surrounding lipids, losing 17% of local lipids may not yield a pore. Actually, this result suggests that a pore might form only if a cell membrane uniformly loses 17% of its entire lipids. Previously, it was found that in order to yield a hole in

DOI: 10.1021/acsnano.7b07005
ACS Nano 2017, 11, 12615−12623

the membrane, a graphene nanosheet should be large enough or multiple small graphene nanosheets are required.[29]

After the pore formation, because of the continuous lipid extraction (Figure 2), ionic currents increased accordingly (Figure 3). Thus, at this stage, the measured current is proportional to the rate of lipid-extraction, that is, $I \approx dN/dt$. In Sim-1, the current increased to a larger value (~1 nA) than the one in Sim-2, because more lipids were extracted and thus a larger hole was formed in the membrane in Sim-1 at the end of simulation. It can be expected that, given more simulation time, all lipids near the graphene nanosheet could be extracted and the hole in the membrane could grow larger. Eventually, direct interactions between lipids in the membrane and the graphene nanosheet become impossible, which yields a saturated ionic current.

To highlight the pore formation process, we calculated the number of water molecules that entered the membrane and were present in a 5-Å-thick layer near the bilayer interface, or the overlap region of the lipid tails in both upper and lower layers (*e.g.*, 5 Å < z < 10 Å). Generally, a water molecule can stay near the headgroup of a lipid but can only temporally enter the hydrophobic lipid-tail region in the membrane. By selecting water molecules found deeply inside the membrane, we calculated the number of water molecules N_W that contributed to the hole formation. In each simulation, N_W fluctuates near zero in the beginning, indicating that water can only temporally enter the already damaged membrane (due to lipid extraction). Similar to the onset of ionic currents, N_W increased sharply after the critical point in each simulation. This avalanche-like process in membrane rupture accompanied by water infiltration is very similar to many phenomena signified with a first-order phase transition.

Noticeably, the following behaviors of $N_W(t)$ as shown in Figure 4a resemble those for $I(t)$ very well (Figure 3). Due to the same thickness (for the calculated water slab), the calculated number of water molecules is proportional to the cross-sectional area of a hole in the lipid membrane. Given the water density (~0.0334 Å^{-3}) for the TIP3P water model, estimated cross-sectional areas for membrane holes at the end of Sim-1 and Sim-2 are 14.4 and 10.8 nm^2, respectively. The ionic current is also proportional to the cross-sectional area of the hole; therefore the time-dependency of N_W is similar to that for the ionic current I.

Figure 4b illustrates a snapshot of the simulation system at the end of Sim-2, showing a water-filled hole in the lipid membrane, connecting both *cis* and *trans* fluidic chambers. The hole resides at one side of the graphene nanosheet, while the membrane on the other side of the nanosheet was not broken yet. Due to water infiltration, lipids near the hole edge reoriented their head groups toward water inside the hole, preventing the exposure of hydrophobic lipid tails to water. Several ions in the emerging aqueous hole can be discerned, and in the externally applied electric field they moved through the hole (*e.g.*, Cl^- from *cis* to *trans* chambers), contributing to the above-mentioned ionic current.

As stated above, a membrane hole can form only after about 17% of the lipids in a membrane patch were extracted onto the graphene nanosheet. Thus, it is interesting to know how the lipid bilayer structure was affected before forming a hole. Because of the constant membrane area inside the solid-state nanopore, the lipid density is expected to reduce after the lipid extraction process started. From the simulation trajectories, we found that the density of the head groups of the lipids

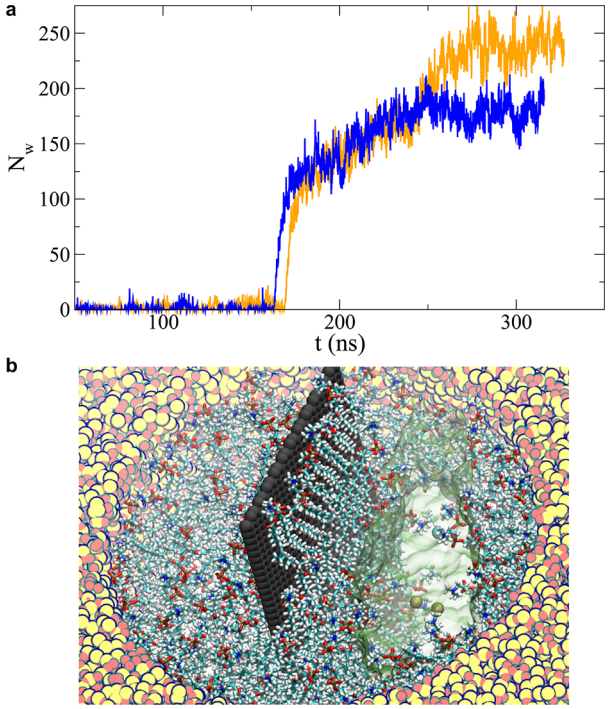

Figure 4. Interactions between water and the POPC membrane. (a) Time-dependent numbers of water molecules inside the membrane during the Sim-1 and the Sim-2. (b) A snapshot of the damaged membrane with a water-filled hole. POPC lipids are in stick representation; atoms in the graphene nanosheet are shown as van der Waals spheres. Water inside the hole is shown transparently with green surface; K^+ and Cl^- are represented as tan and cyan balls; water and ions outside the hole are not shown for clarity.

decreased with time but the density of the tail region remained nearly constant. The latter actually resulted from the enhanced overlap of flexible lipid-tails between the upper and the lower layers (with reduced bilayer thickness). In Figure 5a, we show the time-dependent thickness of the membrane, which was defined as the distance (projected on z axis) between the center of mass (COM) of the phosphorus atoms in the upper layer and the COM of the phosphorus atoms in the lower layer. During the simulation time, the membrane thickness continued to decrease from about 39 Å to about 31 Å on average. Near the time when the hole started to form in the membrane, its thickness was only about 33 Å. The side view of the membrane (see insets in Figure 5a) shows the significant interpenetration of lipid tails between upper and lower layers.

This membrane-thinning effect enables more water molecules to be present at each membrane surface because of the lower lipid density. Additionally, water molecules can further diffuse more deeply into the hydrophobic tail region. The overlap region of the lipid tails was the last barrier before water penetrated the entire membrane. As shown in Figure 4a, water molecules can only temporarily stay in that region, that is, N_W fluctuates around zero, before the hole formation.

As the lipid density decreased further, water molecules can finally penetrate the overlap region. Right after that, the membrane burst and a hole started to develop on the membrane. Consistent with calculated current signals (Figure 3) or number of water molecules inside the membrane (Figure 4a), the hole size increased very quickly (within a few nanoseconds), as shown in Movie S1. Thus, the initial increase of the hole size must result from the rearrangement of lipids

DOI: 10.1021/acsnano.7b07005
ACS Nano 2017, 11, 12615−12623

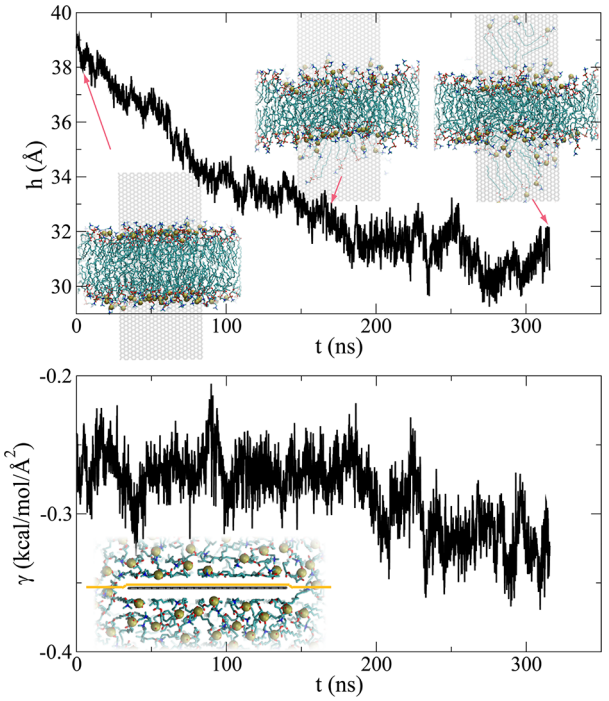

Figure 5. (a) Time-dependent membrane thicknesses in Sim-2. Insets show snap-shots of side-views of the POPC membrane at different times. (b) Time-dependent interfacial interaction energies during the simulation. In the insets the orange line shows where the interface is (the top view). In panels a and b, the graphene nanosheet is in gray; POPC lipids are in stick representation; phosphorus atoms in POPC lipids are shown as tan spheres.

after the burst. To confirm this, we calculated the interfacial interaction energy E between the lipids on both sides of the graphene nanosheet (see inset of Figure 5b); the graphene nanosheet was included into one of the two lipid groups. Both electrostatic (relative dielectric constant = 4) and van der Waals energies were computed, and the latter was found to be dominant. To account for the membrane thickness (h) variation, we define energy density $\gamma = E/A$, where the interfacial area $A = hd$, where d is the width of the graphene nanosheet. As shown in Figure 5b, before the membrane burst, γ was about −0.28 kcal/(mol/Å^2) on average. After the burst, γ was reduced to about −0.33 kcal/(mol/Å^2), indicating that the interaction per unit area became stronger. After the burst, the following increase of the hole area was accompanied by more intimate contacts between the lipids on the hole-forming side and the graphene nanosheet (see Figure 4b), which accounts for the stronger van der Waals attraction inside the membrane. It is noted that the hole was formed at around 160 ns, while the values of γ were saturated after 240 ns. Here, the delay (tens of nanoseconds) indicates the rearrangement of lipids in the remaining membrane after the burst.

We further analyzed the interaction forces exerted on the graphene nanosheet from the membrane lipids on both sides. To exclude the extracted lipids and effects of water on the membrane surface, we only included the inner 30-Å-thick membrane (−15 Å < z < 15 Å in Sim-2) from which forces on the graphene nanosheet were exerted. Because of the charge-neutral atoms in the graphene nanosheet, only van der Waals forces were calculated. Figure 6a,b shows the forces on the graphene nanosheet from the hole-forming side and the non-hole-forming side (see Figure 4b) of the membrane,

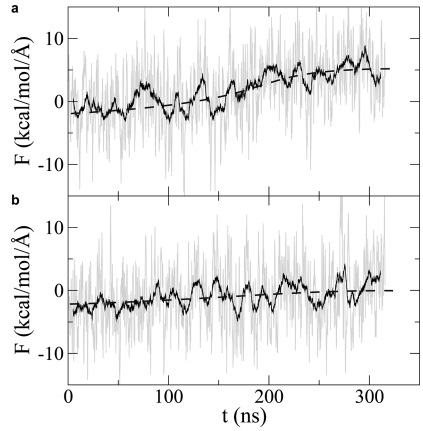

Figure 6. Normal forces on graphene exerted from POPC lipids from the hole-forming side (a) and the non-hole-forming side (b). Gray lines, data averaged over 1 ns; black lines, data averaged over 10 ns; dashed lines, guides to the eye.

respectively. At the beginning, forces on both sides of the nanosheet were negative, suggesting that the membrane was initially under the tension. The tensile force F is about 2 kcal/(mol/Å) initially. The resulting local surface tension estimated by F/d is about 7 dyn/cm. The surface tension of an entire membrane should include the lipid−lipid interaction across the graphene nanosheet as well and is generally about tens of dynes per centimeter.[34] Here, we use the surface tension on the graphene nanosheet to elucidate the nanomechanics during the membrane burst.

With more lipids extracted onto the graphene nanosheet, the tensile force decreased gradually. Note that if this process or deformation is elastic, the force is expected to increase. As described above, the bilayers in the membrane rearranged themselves by allowing the lipid-tails to overlap more to compensate the loss of lipids, which maintains the tensile force. Therefore, such deformation is plastic in nature. At the time of membrane burst (∼160 ns), the tensile force from the membrane on the hole-forming side decreased to zero. The remaining membrane on this side of the graphene nanosheet lost its internal tension. However, on the non-hole-forming side, there remained small tensile forces.

After the burst of membrane, surprisingly, forces exerted from the hole-forming side became positive, that is, repulsive forces, between the graphene nanosheet and nearby membrane lipids. In fact, this nonintuitive result can be understood by considering a balancing force: the hydrophobic force that pushes the lipids against the graphene nanosheet. As shown in Figure 4b, after water's entry into the membrane, such hydrophobic force between the graphene nanosheet and lipids occurred and was normal to the graphene surface. Water's penetration into the lipid membrane was reversible before the loss of a significant amount of lipids (Figure 4a). However, when more water molecules were temporarily present inside the membrane, they yielded hydrophobic force to push the lipids toward the graphene nanosheet, which further allowed more water molecules to get into the membrane. Therefore, this positive feedback loop eventually initiated the avalanche-like process: hole formation. On the non-hole-forming side of the graphene nanosheet, the tensile force in the membrane continued decreasing after the membrane burst and was about zero at around 240 ns. As mentioned above, this time delay is due to the required time (∼80 ns) for the lipids to rearrange

DOI: 10.1021/acsnano.7b07005
ACS Nano 2017, 11, 12615−12623

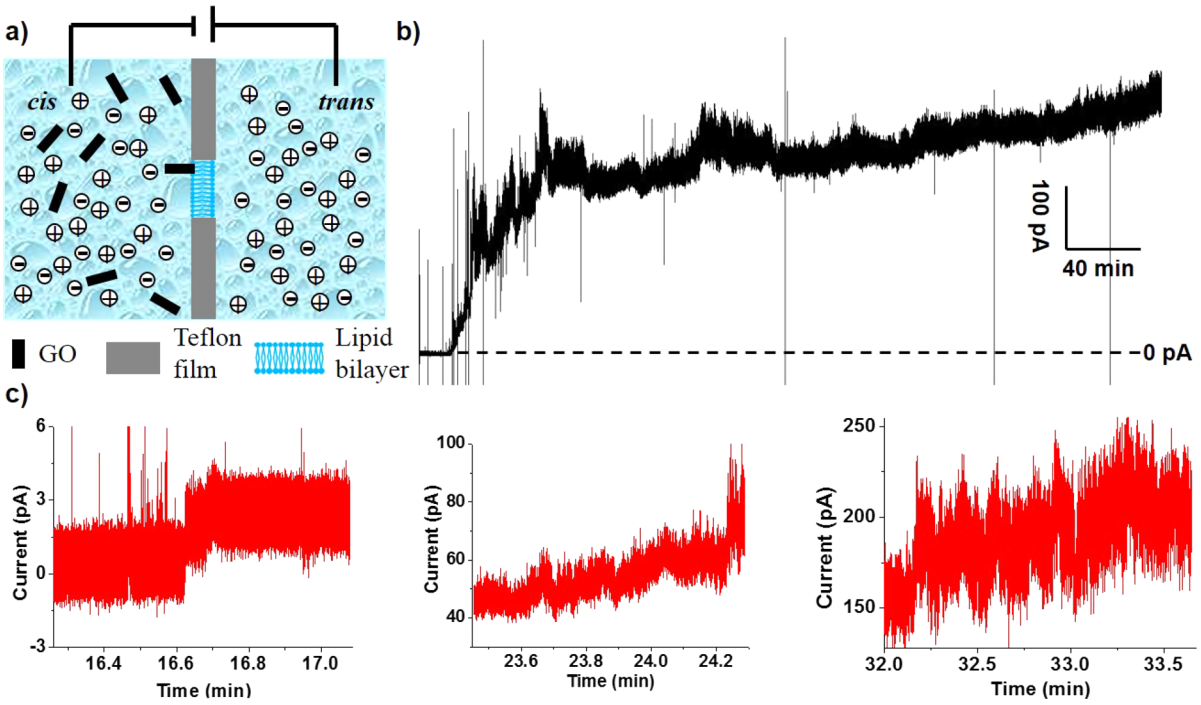

Figure 7. Experimental studies on interactions between GO and the lipid bilayer confined in an orifice. (a) Schematic illustration of the experimental setup (not drawn to scale). (b, c) Ionic currents in the presence of 15 μg/mL GO: (b) 400 min current recording and (c) typical magnified trace segments. The experiment was performed at +20 mV with the lipid bilayer formed at a 156-μm-diameter orifice on a Teflon film. The electrolyte solution contains 1 M NaCl and 10 mM Tris·HCl (pH 7.5).

after the membrane burst on the other side of the graphene nanosheet.

Once a hole is formed in a live cell membrane, depending on the competition between lipid extraction and self-repairing (because of the diffusion of surrounding lipids to fill the hole), the hole size may increase or decrease. However, due to the presence of transmembrane proteins in a live cell membrane, driven or diffusive motions of lipids toward the hole can be hindered.[35] Thus, lipid extraction may dominate the self-repairing, which yields a hole enlargement (similar to the case in our simulation). Alternatively, when the cell membrane is interacting with multiple nanomaterials,[29] it becomes more challenging for self-repair and easier for hole formation. Additionally, many nanomaterials (such as cationic quantum dots) other than graphene nanosheets can passively diffuse through a cell membrane; the cell membrane is only transiently broken and can be repaired by itself.[36] Experimental studies of vesicle−graphene interactions also revealed a transient leakage of dyes inside the vesicle.[17] The typical time scale for these transient membrane holes is around a few milliseconds,[37] which can be adequately detected by measuring the transmembrane current from *cis* to *trans* chambers.[18]

To further validate our simulation results, we carried out a series of experiments to explore the interaction between graphene and the lipid bilayer. Figure 7a illustrates the experimental setup. Briefly, 5 μg/mL graphene oxide (GO) was added and stirred in the chamber after the formation of a lipid bilayer in an orifice on a Teflon film. Here, due to the poor solubility of graphene nanosheets, we used GO nanosheets in our experiment, which contain many unoxidized graphene (sp^2) domains. As shown in our previous simulation and experiments,[12] these large sp^2 domains behave just like pristine graphene and agree well with the theoretical predictions using pure graphene. When applying a lower concentration (5 μg/mL) of GO, the ionic current remained at 0 pA for 20 min (Figure S3 in Supporting Information), suggesting a stable and unbroken lipid bilayer. However, after increasing the GO concentration to 15 μg/mL in the chamber, the ionic current began to fluctuate significantly around 16 min (Figure 7b), indicating that due to the strong interaction GO nanosheets started to breach the membrane. During the next 50 min, the ionic current quickly went up to 350 pA (Figure 7b), suggesting that the continuous lipid extraction had passed the critical point ($t \approx 16.6$ min) and the pore formation in the lipid bilayer became possible. The observed concentration dependency confirms the simulation result that the membrane has to lose a significant amount of lipids before the pore formation either by a large graphene nanosheet or by multiple small ones. Because of this mechanism of pore formation, with limited GO nanosheets inserted in the membrane, the produced pore size may not be proportional to the size of entire membrane. The proportionality occurs only when a significantly large amount of GO nanosheets are in the membrane.

Given that the size (diameter <3 μm) of each GO nanosheet is much smaller than the pore size, multiple GO nanosheets can be present in the membrane when increasing the GO concentration to 15 μg/mL. Figure 7c highlights several representative current signals showing stepwise increases, each of which might signal the formation of an additional pore in the membrane by an inserted GO nanosheet. Similarly, this phenomenon occurs when recording the ionic current through a membrane with multiple protein channels (*e.g.*, α-hemolysin) inserted one-by-one. After that, without any additional pore formation, the ionic current continuously and gradually increased to 420 pA (Figure 7b) because the size of each pore became larger after more lipids were extracted by GO nanosheets. Finally, the current became stable and saturated, after the GO nanosheets were fully covered with the exacted

DOI: 10.1021/acsnano.7b07005
ACS Nano 2017, 11, 12615−12623

lipids. In an independent experiment (see Figure S4), we reproduced the phenomenon of the current increase after the GO-membrane interaction. Overall, these experimental observations are consistent with the simulation results above.

It is worth emphasizing that the phenomenon of lipid extraction is independent of the lipid type, because the extraction is driven by the favorable dispersive interaction between lipid tails and the graphene nanosheet. For two lipid types, POPC (used in our simulation) and DPhPC (used in our experiment), the free energy change for moving a lipid from the membrane to the graphene surface is, respectively, −7.4 kcal/mol[28] and −7.5 kcal/mol (see Figure S5 in Supporting Information). The same phenomenon was previously observed[12] for other types lipids such as POPE, POPE/POPG (3:1), and DPPC. Because the headgroup of a lipid is not involved in the lipid extraction process, even charged lipids (*e.g.*, POPG) can be extracted to the graphene surface.[12]

Generally, the hole formation by nanomaterials can be toxic (*e.g.*, intracellular substance loss) to a biological cell, which as shown above can be detected by measuring the transmembrane ionic current. In many cases, it is possible that some nanomaterials (*e.g.*, TiO_2[38]) are only adsorbed on the membrane surface, and their entry into a cell depends on the following endocytosis process. Although the method proposed above (by measuring DC currents) cannot capture the adsorption of nanomaterials on the membrane, it is possible to apply alternating biasing voltages $V(t)$ to measure the AC signals, that is, $I = C\,dV/dt$ where C is the capacitance of the lipid membrane. Under alternating biasing voltages, each side of the membrane is alternatively charged by K^+ and Cl^- ions and both sides of the membrane are always oppositely charged, yielding a well-defined capacitance. Once nanomaterials are adsorbed on the membrane, the ionic distribution (electric double layer) near the membrane will be affected by the presence of nanomaterials, which results in a different capacitance and consequently a different AC current. Additionally, considering that the capacitance $C = \epsilon S/h$ where ϵ is the dielectric constant, S is the cross-sectional area of the membrane, and h is the membrane thickness, the membrane thinning effect (Figure 5a) before the burst can cause an increase in the capacitance and the consequent AC current. Therefore, while not demonstrated in our simulation, we expect that AC signals might provide more information on particle−membrane interactions.

CONCLUSION

In summary, we have proposed a low-cost yet efficient *in vitro* method to assess the nanotoxicity of nanomaterials toward the cell membrane. By measuring the ionic currents through a cell membrane supported in a solid-state nanopore, it is possible to detect the adverse particle−membrane interactions in real time. Generally, by measuring both DC and AC currents, phenomena such as particle adsorption, membrane thinning, and hole formation can be directly inferred. Here, we demonstrate that once a graphene nanosheet extracted about 17% of the lipids in the membrane and allowed water to penetrate into the membrane, a hole can occur on the membrane, accompanied by an increase in measured ion currents. We analyzed the energetics and nanomechanics during the membrane burst and the hole formation processes and revealed the important role of water. Other mechanisms of pore formation can be dependent on surface properties of a nanomaterial, such as the curvature, polarity, and roughness.[15]

Besides detecting toxicity of a nanomaterial, it can be used to screen designed chemical modifications of an engineered nanomaterial and determine the most biocompatible one. Additionally, the efficiency of antimicrobial peptides/polymers can be conveniently tested and optimized toward bacterial membranes under certain conditions (such as the Ca^{2+}-rich environment[39]). Broadly defined, nanomaterials/nanoparticles are not restricted to the engineered ones but can also include protein toxins, bacteria, or viruses that bind the cell membrane as the precursor of their invasion. Therefore, the nanopore platform described here provides a simple yet powerful means to study broad particle−membrane interactions in general.

METHODS

Molecular Dynamics Simulations. All MD simulations were carried out using the software package NAMD2.9.[40] The entire simulation system measures about 140 × 140 × 160 Å^3, after minimization for 10 ps and equilibration for 5 ns in the NPT ensemble ($P \approx 1$ bar and $T \approx 300$ K). Subsequent production runs were carried out in the NVT ensemble with the electric field turned on. We applied periodic boundary conditions (PBC) in all three dimensions. Long-range Coulomb interactions are computed using particle-mesh Ewald (PME) full electrostatics with the grid size set around 1 Å in each dimension. The van der Waals (vdW) energies between atoms were calculated using a smooth (10−12 Å) cutoff. The temperature T was maintained at 300 K using the Langevin thermostat[41] to all atoms in the SiO_2 membrane. The pressure was kept constant at 1 bar using the Nosé−Hoover method.[42] With the SETTLE algorithm[43] enabled for all bonds, the simulation time-step was 2 fs for bonded and nonbonded (*e.g.*, vdW, angle, and dihedral) interactions, and long-range electric interactions were calculated every 4 fs. During the simulation for melting and quenching the SiO_2 solid, the BKS force field[44] was applied for the amorphous SiO_2 nanopore. We used the TIP3P model[45,46] for water and the standard ion force field[47] and silica force field for the solid membrane interacting with biomolecules.[48] The force field for the graphene nanosheet was adopted from our previous study;[12] the CHARMM force field[32] was used for POPC lipids.

Materials and Reagents. The graphene oxide (GO) was purchased from Chengdu Organic Chemicals Co. Ltd., Chinese Academy of Sciences (Chengdu, China). The size (diameter) of each GO nanosheet varies from 0.5 to 3 μm. The lipid, 1,2-diphytanoylphosphatidylcholine (DPhPC), was purchased from Avanti Polar Lipids (Alabaster, AL). All the other chemicals were obtained from Sigma-Aldrich (St. Louis, MO)).

Bilayer Experiment and Electrical Recording. The bilayer experiments were performed in a planar bilayer chamber, which was separated into two compartments by a Teflon film, and the lipid bilayer was formed at a 156-μm-diameter aperture of the Teflon film using DPhPC according to the Montal−Mueller method.[49] All the experiments were carried out in the chamber with 2 mL of buffer solutions added in each compartment containing 1 M NaCl and 10 mM Tris-HCl (pH 7.5). The higher ion concentration than the one (0.15 M) used in simulation can enhance the ionic current through the pore[50] achieving improved signal-to-noise ratios and meanwhile can screen charges of membrane/GO at pH 7.5. GO nanosheets were added to the grounded *cis* compartment. An Axopatch 200B amplifier (Molecular Devices, Sunnyvale, CA) was used to record the ionic currents that were low-pass filtered with a built-in four-pole Bessel filter at 2 kHz and sampled at 50 kHz by a computer equipped with a Digidata 1440A converter (Molecular Devices).

ASSOCIATED CONTENT

Supporting Information

The Supporting Information is available free of charge on the ACS Publications website at DOI: 10.1021/acsnano.7b07005.

DOI: 10.1021/acsnano.7b07005
ACS Nano 2017, 11, 12615−12623

Top view of graphene in the lipid membrane, deformation of the lipid membrane around the inserted graphene (side views), current traces from experiment, and illustration of an annihilation process of a DPhPC lipid in the lipid bilayer or on the graphene surface (PDF)

Hole-forming process in the lipid membrane after excessive lipid-extraction onto the graphene nanosheet (Sim-1) (MPG)

AUTHOR INFORMATION

Corresponding Authors

*E-mail: bluan@us.ibm.com.
*E-mail: ruhongz@us.ibm.com.

ORCID

Binquan Luan: 0000-0002-9414-5379
Ruhong Zhou: 0000-0001-8624-5591

Notes

The authors declare no competing financial interest.

ACKNOWLEDGMENTS

The authors thank Tien Huynh for his help with proofreading the manuscript. We also gratefully acknowledge the financial support from the IBM Bluegene Science Program (Grant Numbers W125859, W1464125, and W1464164).

REFERENCES

(1) Song, L.; Hobaugh, M. R.; Shustak, C.; Cheley, S.; Bayley, H.; Gouaux, J. E. Structure of Staphylococcal α-Hemolysin, a Heptameric Transmembrane Pore. *Science* **1996**, *274*, 1859−1865.

(2) Dal Peraro, M.; Van Der Goot, F. G. Pore-Forming Toxins: Ancient, but never Really out of Fashion. *Nat. Rev. Microbiol.* **2016**, *14*, 77−92.

(3) Bode, D. C.; Baker, M. D.; Viles, J. H. Ion Channel Formation by Amyloid-β42 Oligomers but not Amyloid-β40 in Cellular Membranes. *J. Biol. Chem.* **2017**, *292*, 1404.

(4) Di Scala, C.; Yahi, N.; Boutemeur, S.; Flores, A.; Rodriguez, L.; Chahinian, H.; Fantini, J. Common Molecular Mechanism of Amyloid Pore Formation by Alzheimer's β-Amyloid Peptide and α-Synuclein. *Sci. Rep.* **2016**, *6*, 28781.

(5) Brogden, K. A. Antimicrobial Peptides: Pore Formers or Metabolic Inhibitors in Bacteria? *Nat. Rev. Microbiol.* **2005**, *3*, 238−250.

(6) Yang, L.; Gordon, V. D.; Trinkle, D. R.; Schmidt, N. W.; Davis, M. A.; DeVries, C.; Som, A.; Cronan, J. E.; Tew, G. N.; Wong, G. C. Mechanism of a Prototypical Synthetic Membrane-Active Antimicrobial: Efficient Hole-Punching *via* Interaction with Negative Intrinsic Curvature Lipids. *Proc. Natl. Acad. Sci. U. S. A.* **2008**, *105*, 20595−20600.

(7) Nederberg, F.; Zhang, Y.; Tan, J. P.; Xu, K.; Wang, H.; Yang, C.; Gao, S.; Guo, X. D.; Fukushima, K.; Li, L.; Hedrick, J.; Yang, Y. Biodegradable Nanostructures with Selective Lysis of Microbial Membranes. *Nat. Chem.* **2011**, *3*, 409−414.

(8) Nel, A.; Xia, T.; Mädler, L.; Li, N. Toxic Potential of Materials at the Nanolevel. *Science* **2006**, *311*, 622−627.

(9) Shang, L.; Nienhaus, K.; Nienhaus, G. U. Engineered Nanoparticles Interacting with Cells: Size Matters. *J. Nanobiotechnol.* **2014**, *12*, 5.

(10) Guo, Y.; Terazzi, E.; Seemann, R.; Fleury, J. B.; Baulin, V. A. Direct Proof of Spontaneous Translocation of Lipid-Covered Hydrophobic Nanoparticles through a Phospholipid Bilayer. *Sci. Adv.* **2016**, *2*, e1600261.

(11) Bailey, C. M.; Kamaloo, E.; Waterman, K. L.; Wang, K. F.; Nagarajan, R.; Camesano, T. A. Size Dependence of Gold Nanoparticle Interactions with a Supported Lipid Bilayer: A QCM-D Study. *Biophys. Chem.* **2015**, *203*, 51−61.

(12) Tu, Y.; Lv, M.; Xiu, P.; Huynh, T.; Zhang, M.; Castelli, M.; Liu, Z.; Huang, Q.; Fan, C.; Fang, H.; Zhou, R. Destructive Extraction of Phospholipids from Escherichia Coli Membranes by Graphene Nanosheets. *Nat. Nanotechnol.* **2013**, *8*, 594−601.

(13) Li, Y.; Yuan, H.; von dem Bussche, A.; Creighton, M.; Hurt, R. H.; Kane, A. B.; Gao, H. Graphene Microsheets Enter Cells through Spontaneous Membrane Penetration at Edge Asperities and Corner Sites. *Proc. Natl. Acad. Sci. U. S. A.* **2013**, *110*, 12295−12300.

(14) Castellana, E. T.; Cremer, P. S. Solid Supported Lipid Bilayers: From Biophysical Studies to Sensor Design. *Surf. Sci. Rep.* **2006**, *61*, 429−444.

(15) Roiter, Y.; Ornatska, M.; Rammohan, A. R.; Balakrishnan, J.; Heine, D. R.; Minko, S. Interaction of Nanoparticles with Lipid Membrane. *Nano Lett.* **2008**, *8*, 941−944.

(16) Yi, P.; Chen, K. L. Release Kinetics of Multiwalled Carbon Nanotubes Deposited on Silica Surfaces: Quartz Crystal Microbalance with Dissipation (QCM-D) Measurements and Modeling. *Environ. Sci. Technol.* **2014**, *48*, 4406−4413.

(17) Liu, X.; Chen, K. L. Interactions of Graphene Oxide with Model Cell Membranes: Probing Nanoparticle Attachment and Lipid Bilayer Disruption. *Langmuir* **2015**, *31*, 12076−12086.

(18) Branton, D.; Deamer, D.; Marziali, A.; Bayley, H.; Benner, S.; Butler, T.; Di Ventra, M.; Garaj, S.; Hibbs, A.; Huang, X.; Jovanovich, S.; Krstic, P.; Lindsay, S.; Ling, X.; Mastrangelo, C.; Meller, A.; Oliver, J.; Pershin, Y.; Ramsey, J.; Riehn, R.; et al. The Potential and Challenges of Nanopore Sequencing. *Nat. Biotechnol.* **2008**, *26*, 1146−1153.

(19) Yusko, E. C.; Bruhn, B. R.; Eggenberger, O. M.; Houghtaling, J.; Rollings, R. C.; Walsh, N. C.; Nandivada, S.; Pindrus, M.; Hall, A. R.; Sept, D.; Li, J.; Kalonia, D.; Mayer, M. Real-Time Shape Approximation and Fingerprinting of Single Proteins Using a Nanopore. *Nat. Nanotechnol.* **2017**, *12*, 360−367.

(20) Zhou, R.; Huang, X.; Margulis, C.; Berne, B. Hydrophobic Collapse in Multidomain Protein Folding. *Science* **2004**, *305*, 1605.

(21) Luan, B.; Huynh, T.; Zhao, L.; Zhou, R. Potential Toxicity of Graphene to Cell Functions via Disrupting Protein-Protein Interactions. *ACS Nano* **2015**, *9*, 663−669.

(22) Liu, P.; Huang, X.; Zhou, R.; Berne, B. Observation of a Dewetting Transition in the Collapse of the Melittin Tetramer. *Nature* **2005**, *437*, 159−162.

(23) Stirnemann, G.; Kang, S.-g.; Zhou, R.; Berne, B. J. How Force Unfolding Differs from Chemical Denaturation. *Proc. Natl. Acad. Sci. U. S. A.* **2014**, *111*, 3413−3418.

(24) Li, J.; Gong, X.; Lu, H.; Li, D.; Fang, H.; Zhou, R. Electrostatic Gating of a Nanometer Water Channel. *Proc. Natl. Acad. Sci. U. S. A.* **2007**, *104*, 3687−3692.

(25) Luan, B.; Robbins, M. O. The Breakdown of Continuum Models for Mechanical Contacts. *Nature* **2005**, *435*, 929−932.

(26) Tu, Y.; Xiu, P.; Wan, R.; Hu, J.; Zhou, R.; Fang, H. Water-Mediated Signal Multiplication with Y-shaped Carbon Nanotubes. *Proc. Natl. Acad. Sci. U. S. A.* **2009**, *106*, 18120−18124.

(27) Luan, B.; Peng, H.; Polonsky, S.; Rossnagel, S.; Stolovitzky, G.; Martyna, G. Base-by-Base Ratcheting of Single Stranded DNA through a Solid-State Nanopore. *Phys. Rev. Lett.* **2010**, *104*, 238103.

(28) Luan, B.; Huynh, T.; Zhou, R. Complete Wetting of Graphene by Biological Lipids. *Nanoscale* **2016**, *8*, 5750−5754.

(29) Duan, G.; Zhang, Y.; Luan, B.; Weber, J. K.; Zhou, R. W.; Yang, Z.; Zhao, L.; Xu, J.; Luo, J.; Zhou, R. H. Graphene-Induced Pore Formation on Cell Membranes. *Sci. Rep.* **2017**, *7*, 42767.

(30) Rascol, E.; Devoisselle, J.-M.; Chopineau, J. The Relevance of Membrane Models to Understand Nanoparticles-Cell Membrane Interactions. *Nanoscale* **2016**, *8*, 4780−4798.

(31) Kučerka, N.; Tristram-Nagle, S.; Nagle, J. F. Structure of Fully Hydrated Fluid Phase Lipid Bilayers with Monounsaturated Chains. *J. Membr. Biol.* **2006**, *208*, 193−202.

(32) Klauda, J. B.; Venable, R. M.; Freites, J. A.; O'Connor, J. W.; Tobias, D. J.; Mondragon-Ramirez, C.; Vorobyov, I.; MacKerell, A. D.,

DOI: 10.1021/acsnano.7b07005
ACS Nano 2017, 11, 12615−12623

Jr; Pastor, R. W. Update of the CHARMM All-Atom Additive Force Field for Lipids: Validation on Six Lipid Types. *J. Phys. Chem. B* **2010**, *114*, 7830−7843.
(33) Tarek, M. Membrane Electroporation: a Molecular Dynamics Simulation. *Biophys. J.* **2005**, *88*, 4045−4053.
(34) Gullingsrud, J.; Schulten, K. Lipid Bilayer Pressure Profiles and Mechanosensitive Channel Gating. *Biophys. J.* **2004**, *86*, 3496−3509.
(35) Goose, J. E.; Sansom, M. S. Reduced Lateral Mobility of Lipids and Proteins in Crowded Membranes. *PLoS Comput. Biol.* **2013**, *9*, e1003033.
(36) Verma, A.; Uzun, O.; Hu, Y.; Hu, Y.; Han, H.-S.; Watson, N.; Chen, S.; Irvine, D. J.; Stellacci, F. Surface-Structure-Regulated Cell-membrane Penetration by Monolayer-Protected Nanoparticles. *Nat. Mater.* **2008**, *7*, 588−595.
(37) Dimova, R.; Riske, K. A.; Aranda, S.; Bezlyepkina, N.; Knorr, R. L.; Lipowsky, R. Giant Vesicles in Electric Fields. *Soft Matter* **2007**, *3*, 817−827.
(38) Andersson, P. O.; Lejon, C.; Ekstrand-Hammarström, B.; Akfur, C.; Ahlinder, L.; Bucht, A.; Österlund, L. Polymorph-and Size-Dependent Uptake and Toxicity of TiO_2 Nanoparticles in Living Lung Epithelial Cells. *Small* **2011**, *7*, 514−523.
(39) Luan, B.; Chen, K. L.; Zhou, R. Mechanism of Divalent-Ion-Induced Charge Inversion of Bacterial Membranes. *J. Phys. Chem. Lett.* **2016**, *7*, 2434−2438.
(40) Phillips, J. C.; Braun, R.; Wang, W.; Gumbart, J.; Tajkhorshid, E.; Villa, E.; Chipot, C.; Skeel, R. D.; Kale, L.; Schulten, K. Scalable Molecular Dynamics with NAMD. *J. Comput. Chem.* **2005**, *26*, 1781−1802.
(41) Allen, M. P.; Tildesley, D. J. *Computer Simulation of Liquids*; Oxford University Press: New York, 1987.
(42) Martyna, G. J.; Tobias, D. J.; Klein, M. L. Constant Pressure Molecular Dynamics Algorithms. *J. Chem. Phys.* **1994**, *101*, 4177−4189.
(43) Miyamoto, S.; Kollman, P. A. SETTLE: An Analytical Version of the SHAKE and RATTLE Algorithm for Rigid Water Molecules. *J. Comput. Chem.* **1992**, *13*, 952−962.
(44) van Beest, B.; Kramer, G.; van Santen, R. Force Fields for Silicas and Aluminophosphates Based on Ab Initio Calculations. *Phys. Rev. Lett.* **1990**, *64*, 1955−1958.
(45) Jorgensen, W. L.; Chandrasekhar, J.; Madura, J. D.; Impey, R. W.; Klein, M. L. Comparison of Simple Potential Functions for Simulating Liquid Water. *J. Chem. Phys.* **1983**, *79*, 926−935.
(46) Neria, E.; Fischer, S.; Karplus, M. Simulation of Activation Free Energies in Molecular Systems. *J. Chem. Phys.* **1996**, *105*, 1902.
(47) Beglov, D.; Roux, B. Finite Representation of an Infinite Bulk System: Solvent Boundary Potential for Computer Simulations. *J. Chem. Phys.* **1994**, *100*, 9050−9063.
(48) Cruz-Chu, E. R.; Aksimentiev, A.; Schulten, K. Water-Silica Force Field for Simulating Nanodevices. *J. Phys. Chem. B* **2006**, *110*, 21497−21508.
(49) Montal, M.; Mueller, P. Formation of Bimolecular Membranes from Lipid Monolayers and a Study of Their Electrical Properties. *Proc. Natl. Acad. Sci. U. S. A.* **1972**, *69*, 3561−3566.
(50) Luan, B.; Stolovitzky, G. An Electro-Hydrodynamics-Based Model for the Ionic Conductivity of Solid-State Nanopores during DNA Translocation. *Nanotechnology* **2013**, *24*, 195702.

DOI: 10.1021/acsnano.7b07005
ACS Nano 2017, 11, 12615−12623